Technologies for Lightweight Structures 1(2) (2017), pp. 197–207
Special issue: 3rd International MERGE Technologies Conference (IMTC), 21st–22nd September 2017, Chemnitz

Technologies for Lightweight Structures

Additive manufacturing of capacitive humidity sensors by screen printing for condition monitoring of FRP composites

Tobias Seifert[1)], Jörg Martin[2)], Thomas Seider[3)] Maik Wiemer[1)], Thomas Otto [2)3)]

[1)] Department System Packaging, info@enas.fraunhofer.de, Fraunhofer Institute for Electronic Nano Systems ENAS, Technology Campus 3, 09126 Chemnitz, Germany

[2)] Department Multi Device Integration, info@enas.fraunhofer.de, Fraunhofer Institute for Electronic Nano Systems ENAS, Technology Campus 3, 09126 Chemnitz, Germany

[3)] Center for Microtechnologies, info@zfm.tu-chemnitz.de, Chemnitz University of Technology, Reichenhainer Straße 70, 09126 Chemnitz, Germany

Keywords

humidity sensors, mass production, printed electronics, screen printing, sensor integration

Abstract

Screen printing as a method of additive manufacturing applicable for the production of highly sensitive humidity sensors is presented. For this purpose, manufacturing, benchmarking and optimization of sensitive micro-composite dielectric paste systems suitable for screen printing are demonstrated. Furthermore, commercially available silver paste systems were rheologically and electrically characterized and benchmarked. Thereby bulk silver conductivities of up to 15 % were measured with average layer thicknesses in the range between 3 - 10 µm and an occurring surface roughness R_a between 0.7 - 3.7 µm. The printed sensors capacitance was measured along with the characterization of its humidity sensing capability. The capacitance of the printed sensors varied between 6.2 - 8.5 pF depending on the layer thickness of the micro-composite dielectric materials and increased up to 26 pF while detecting 90 % relative humidity. Differences between water molecule absorption and desorption are determined by the occurring hysteresis between the detection of increasing and decreasing humidity. Malfunctions of the sensors due to the arising cross contact between top and bottom electrode could be addressed by varying the layer thickness or selection of materials.

1 Introduction

By combining lightweight construction with high mechanical performance, Fiber Reinforced Polymers (FRP) gained attention in industries that are based on structural and civil engineering due to their promising benefits over conventional building materials [1,2]. However, concerns about durability have slowed down the evolution of FRP in new applications. In addition to temperature or energetic radiation, moisture effects caused by humidity, vapors or liquids also have a big impact on the mechanical properties of FRP in chemical, physical and mechanical terms [2]. Moreover, the exposure of FRP to moisture has detrimental effects the performance of FRP such as matrix plasticization, chemical degradation and mechanical degradation [3]. Hence, the detection of humidity is supposed to indicate moisture-related degradation and is dominated by impedance- (resistive) or capacitive-based principles. Several miniaturized humidity sensors with different transduction techniques are available [4]. Although the production of miniaturized humidity sensors by conventional processes delivers precise, low-cost devices with a high-scale throughput, printed film-based humidity sensors with acceptable gasketing, design flexibility and a quick deposition rate promise cost-effectiveness and an especially high potential for the application of sensors in a wide range of processes onto a big variety of substrates [4, 5].

In order to enable condition monitoring of FRP with screen printing, an alternative method of additive manufacturing for flexible capacitive moisture sensors, which are supposed to be directly integrated into FRP, is presented.

Digital Object Identifier: http://dx.doi.org/10.21935/tls.v1i2.104
www.lightweight-structures.de

For the additive manufacturing of humidity sensors several printing technologies are under investigation. Besides the handwriting of sensitive layers based on oxidized multi-walled carbon nanotubes (MWCNT) with ink markers [6], there have already been several approaches of manufacturing capacitive sensors for moisture detection by flexographic printing or spin coating [5]. The successful integration of foil-based sensors into FRP was already shown for fiber-reinforced thermoplastic composites [7].

But digital and maskless printing technologies were also used to manufacture fully printed capacitive humidity sensors with different interdigital electrode geometries [8]. Even the switch to paper as a humidity sensing medium could be demonstrated for the use of 2-step inkjet printable capacitive humidity sensors in a proof-of-concept [9]. With the help of screen printing, remotely readable and flexibly hybrid temperature/humidity sensor pairs could be produced by adding temperature- and humidity-sensitive elements to screen printed antenna coils [10]. However, resistive humidity sensors were also recently produced by combining laser ablation of interdigitated electrodes and screen printing of humidity-sensitive TiO_2 particles [11]. By iterating interdigitated electrode structures and implementing out-of-plane designs, an enhanced sensitivity of the humidity sensors was demonstrated [12].

This work describes the possibilities of manufacturing fully screen printed capacitive humidity sensors on flexible substrates based on humidity-sensitive nano- and microcomposites. For the realization of this application, the manufacturing and printing of the involved materials, the analysis of the rheology of the related materials, the printed morphology and post-processing as well as the characterization of the printed layers are described. Furthermore, the evaluation of the electrical performance of printed layers and the sensing performance of sensor devices are shown. For the evaluation of printing and post-processing results, printed layers and occurring layer interfaces were analyzed using scanning electron microscopy (SEM) and focused ion beam (FIB).

2 Materials and methods

2.1 Layouting and build of capacity humidity sensors

According to the capacitive working principle, a hygroscopic dielectric layer needs to be embedded between a conductive bottom and top electrode. As the dielectric permittivity of water is much larger compared to that of the dielectric layer, adsorbed water causes an increase in permittivity along with an increased capacitance of the sensor. Therefore, a total of three different layers are involved in such a sensor design, which induces the need for three differently designed screen printing screens. These screens are used to successively print the layers on the substrate during three separate and subsequent printing steps. In Fig. 1 the sensor-based screen layout for all three layers is shown in the overlay. The adopted layout provides a throughput of a total of 22 printed devices per substrate.

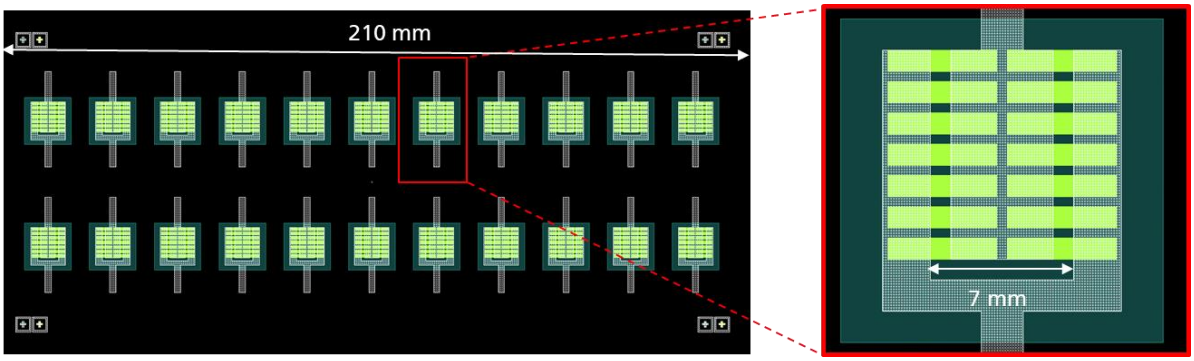

Fig. 1: Layout of screen printing screens with separate layout of bottom electrode (white), micro-composite dielectric layer (olive green) and top-electrode (light green)

2.2 Sensor materials

Two different silver-based paste systems were evaluated for the printing of the top and bottom electrodes. Besides the silver nanoparticle paste Genes'Ink Smart Ink S-CS21303 (Genes'Ink, Rousset, France) (nanoparticle-based, solids content 55±5 wt%, viscosity 4000 - 7000 cP, according to paste data sheet) Sun Chemical AST 6000 (Sun Chemical Corporation, Parsippany, USA) (microparticle-based, solids content 65-70 wt%, viscosity 40000 - 70000 cP, according to paste data sheet) was also

printed as received. As working substrate, standardized polyimide sheets of the type Kapton® (DuPont, Wilmington, USA) with an average thickness of 50 µm were applied during all screen printing tests. A hygroscopic dielectric paste system was customized and manufactured with nanoporous silica particles at an average size of 2 - 25 µm (Sigma Aldrich) and binder polyvinylbutyral (PVB, Pioloform BL 16, Kuraray) solved in butanol (Sigma Aldrich).

2.3 Paste printing, post processing & characterization

The rheological benchmarking was applied at 20 °C platen temperature using a rheometer Anton Paar Physica MCR 301 (Anton Paar, Graz, Austria) in order to correlate the printing results with the rheological properties. The screen printing was performed using a screen printer DEK Horizon 03iX (ASM Assembly Systems GmbH und Co. KG (ASMPT), Munich, Germany). All printing trials were performed in ambient conditions. The printed patterns were post-processed with a thermal treatment using the heating plate and oven Memmert UM 400 (Memmert, Schwabach, Germany). The patterns and sensors were characterized using the light microscope Nikon Eclipse 200 (Nikon Corporation, Tokio, Japan). The cross-sectional profiles were evaluated with the surface profiler Veeco Dektak 150 (Veeco, New York, USA).

2.4 Electrodes and device benchmarking

The electrical characterization of the printed electrodes was performed with a Keithley 2612 SourceMeter (Keithley Instruments, Cleveland, OH, USA) and Süss Microtec probe system (Süss, München, Germany) based on 4-Point test patterns printed on Kapton®.

The performance of the printed composite humidity sensors was investigated in a climatic chamber (KPK 200, Feutron). The capacitance of sensor test samples was recorded with an LCR meter (HM 8118, Rohde & Schwarz HAMEG) while a step-like humidity changing profile was applied to the samples. The target humidity was cycled from 20 % to 90 % and back to 20 % r. h. in steps of 10 %. After each step of increasing or decreasing the humidity, the value was maintained at 90 % r. h. for 20 min or 30 min, respectively, to allow the humidity to stabilize. The chamber temperature was fixed at 30 °C throughout the measurement cycle. Afterwards, the sensor characteristics were extracted from the temporal records of target humidity, measured chamber humidity and capacitance.

3 Results

3.1 Rheological benchmarking of paste systems

The performance of screen printing in terms of printed pattern properties is strongly correlated with the rheology of the paste materials involved [13]. Among other things, static rheological properties like viscosity and thixotropy are critical for the optimization of pastes considered for screen printing applications [14]. Fig. 1 shows the results of flow curve measurements in correlation to the printing performance of respectively sensitive micro-composite dielectric paste systems made of micro-composite materials on the basis of different solid volume contents (v% silica + PVB). In order to determine the printing accuracy, which is represented by edge sharpness, the printing screen, which is supposed to print the sensor's bottom electrode, was used.

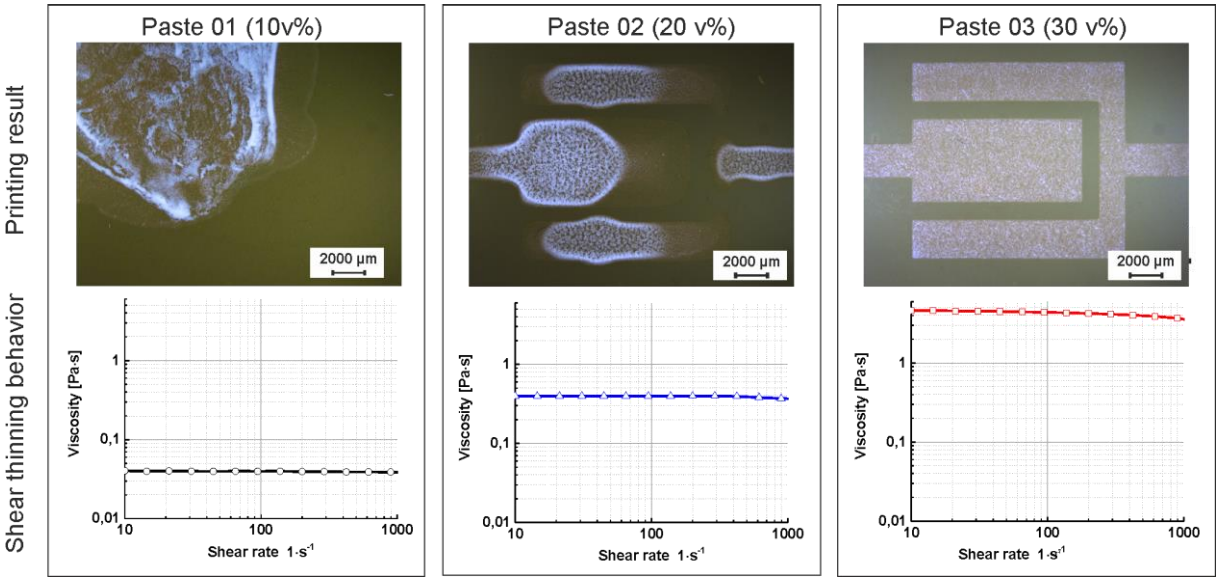

Fig. 2: Results of flow curve measurements in correlation to the printing performance of respectively sensitive dielectric micro-composite pastes based on different solid volume contents v%

It can be seen that the viscosity of the pastes increases with a certain shear rate in the range 10–1000 [$1 \cdot s^{-1}$] in correlation with an increased solid volume content. Furthermore, it becomes clear that the chosen PVB binder system including butanol provides shear thinning properties in combination with silica particles. This effect is imperative for transferring the paste through the printing screen openings during the screen printing process. Additionally, the printing performance improves in terms of printing accuracy with increasing viscosity. This is due to reduced spread of higher viscosity paste systems after transferring the paste through the screen and the subsequent recovery of paste viscosity over a short period of time. This effect is mainly described by the thixotropic behavior of the pastes. As can be seen in Fig. 1, the paste with the highest solid volume content of 30 v% provides the best printing accuracy, which in turn is correlated with a fast recovery of viscosity after finishing the screen printing process. The evaluation of paste rheology not only helps to improve the suitability of pastes for screen printing. It also supports the monitoring of possible variations within the paste manufacturing process itself. This way, possible inconsistencies regarding the involved batches of paste raw materials involved, the weighing process or the mixing setup could be identified. In order to visualize the suitability of the pastes for screen printing in terms of shear thinning and recovery, a dynamic step response test was run for evaluation of pastes thixotropic behavior. The test consists of varying the shear stress stepwise while continuously measuring the viscosity. The phases of different shear rates are inspired by the phases of the screen printing process itself. Including a rest after the deposition on the screen (i), flooding over the screen (ii), printing trough the mesh (iii) and recovery on the substrate (iv), the screen printing process can be separated into four different phases [14]. Here a short rest after phase (ii) with subsequent phases (iii) and (iv) was tested by presenting these three subsequent steps with separately defined pairs of shear rate and duration. The set values for shear rate and duration are shown in Table 1.

Table 1: Phase-dependent set values of shear rate and duration for step response test

Step	**I**	**II**	**III**
Shear rate [1·s^{-1}]	0.1	40	0.1
Duration [s]	60	100	200

With this setup, not only two different batches of sensitive micro-composite dielectric paste were rheologically characterized, but also two commercially available silver paste systems used for printing electrode layers within the humidity sensor setup were benchmarked. In Fig. 3, the comparison of the thixotropic behavior as well as the shear thinning properties of four characterized pastes is presented.

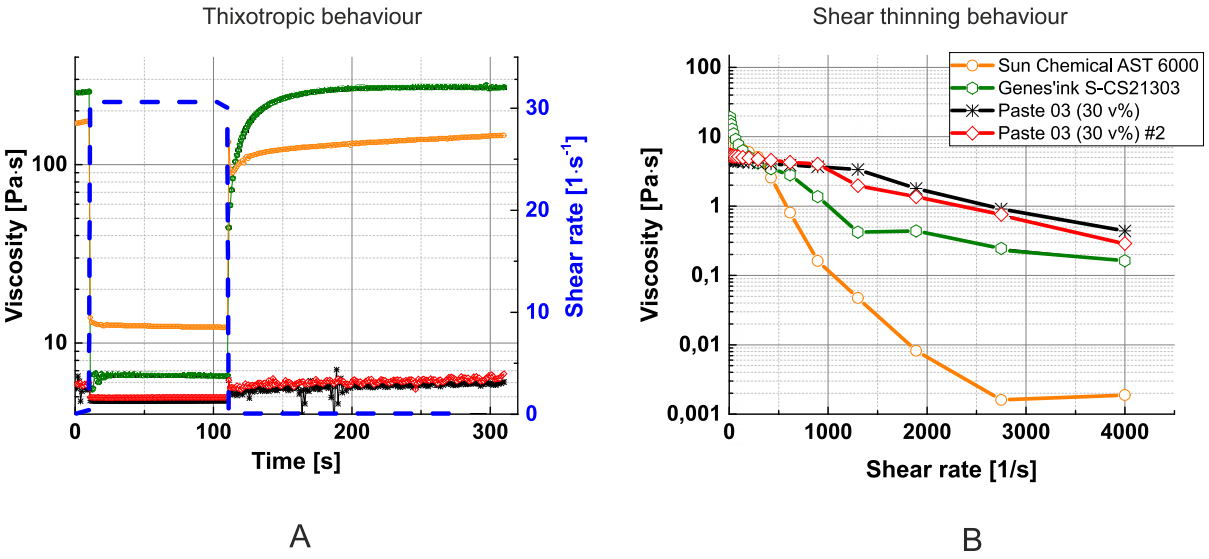

Fig. 3: Measurement results of the thixotropic behavior (A) and the shear thinning behavior (B) of involved paste systems

As can be seen in Fig. 3B, both batches of sensitive micro-composite dielectric pastes provide comparable shear thinning properties. Whereas paste 03 #01 provides a viscosity of 5.46 Pa·s at 10·s^{-1}, the second batch delivered with a viscosity of 4.65 Pa·s values in a narrow range. The shear thinning effect at 4000·s^{-1} with -91% (batch #2) vs. -94 % (batch #1) is also comparable. This results in verified pastes which produce a manufacturing process of rheologically comparable batches for identical mixed paste systems and the general possibility of paste transfer through mesh openings. In contrast, both silver pastes provide stronger thinning effects, whereby Sun Chemical AST 6000 provides a lower viscosity with 9.8 Pa·s at 10·s^{-1} compared to Genes'Ink S-C21303 19 Pa·s at 10·s^{-1}. But the shear thinning effect of Sun Chemical AST 6000 at 4000·s^{-1} with -99.9 % is comparable to Genes'Ink with -99 %. When comparing the thixotropic behavior of the pastes involved, Fig. 3A shows that all pastes exhibit a fast reduction in viscosity when shear rate of 40 ·s^{-1} is applied for 100 s. According to the flow curve analysis, both commercially available paste systems provide stronger reduction in viscosity > 90 %, while both customized paste systems provide a reduction of ~16 % at a given shear rate. However, in the recovery phase, differences between both commercial paste systems are also visible. While Sun Chemical AST 6000 recovers above the original viscosity levels after the shear rate is reset to 0.1 ·s^{-1}, Genes'Ink S-C21303 does not reach the original levels again. This could lead to the conclusion that after printing, Genes'Ink's spread could be higher than Sun Chemical's due to lower resulting paste viscosity after printing. It cannot be ruled out that Sun Chemical AST 6000 may provide higher viscosity levels after recovery due to drying effects during measurement, as no solvent trap was used during measurement. In both customized paste systems, the viscosity recovery exceeds original viscosity values by > 9 %, which generally points not only to a low spread after completion of the printing step is, but also to influencing drying effects during the recovery step. Table 2 shows the measured viscosities of the paste systems involved.

Table 2: Measured viscosities of paste systems during flow curve and thixotropic characterization

	Flow Curve		**Thixotropic behavior**		
	Shear Rate [1·s^{-1}]	**Viscosity [Pa·s]**	**Viscosity I [Pa·s]**	**Viscosity II [Pa·s]**	**Viscosity III [Pa·s]**
AST 6000	10	9.8	254.0	6.6 (-97 %)	271.0 (+7 %)
	4000	0.002 (- 99 %)			
S-C21303	10	19	170.0	12.5 (-93 %)	146.0 (-14 %)
	4000	0.16 (-99 %)			
Paste 03 #1	10	5.46	5.9	4.9 (-17 %)	6.7 (+14 %)
	4000	0.29 (-94 %)			
Paste 03 #2	10	4.65	5.6	4.7 (-16 %)	6.1 (+9 %)
	4000	0.44 (-91 %)			

4 Electrode performance

In order to identify the best performing silver paste for the printing of humidity sensor electrodes, both chosen screen printing paste systems, Sun Chemical AST 6000 and Genes'Ink S-C21303, were electrically characterized. As critical parameter for the electrical characterization, the surface resistance was chosen. Fig. 4 shows the measured surface resistance of both materials with respect to the chosen sintering regime.

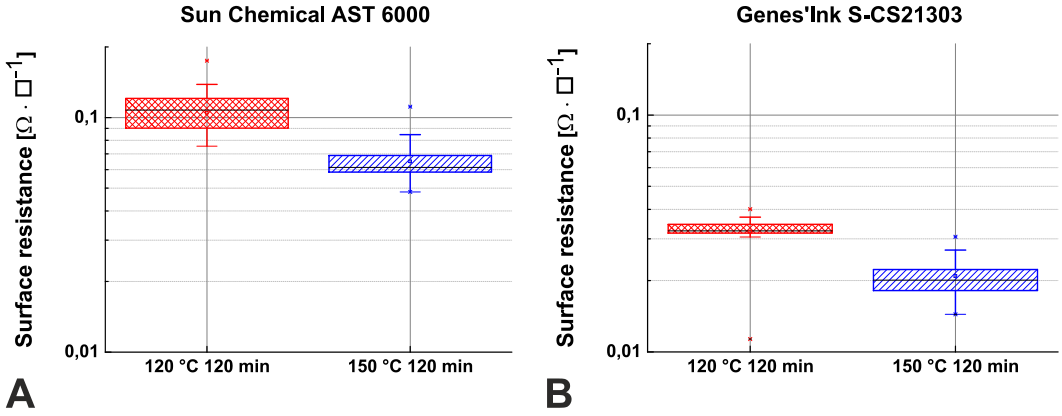

Fig. 4: Measured surface resistance of Sun Chemical AST 6000 (A), Genes'Ink S-CS21303 (B) with respect to the chosen sintering regime

The measured value of the surface resistivity and calculated bulk conductivity compared to silver in % is shown in Table 3. As value for the resistivity of bulk silver ρ_{BS} = 1.58·10^{-8} Ω·m was used. With an average layer thickness of 10 µm, Sun Chemical AST 6000 delivers a greater layer thickness compared to Genes'Ink (5 µm) with the given screen printing setup. At a sintering regime of 120 °C for 120 min, Genes'Ink S-C21303 provides better electrical performance with a surface resistance of 0.03 ± 0.005 Ω·□$^{-1}$ compared to Sun Chemical AST 6000 with a measured surface resistance of 0.10 ± 0.035 Ω·□$^{-1}$. After increasing the sintering temperature at constant sintering time, the surface resistance of both silver pastes could be reduced. As a result, Genes'Ink S-C21303 again performed better with a lower surface resistivity compared to Sun Chemical. In summary, at the chosen sintering setup with a curing time of 120 min and a curing temperature of 150 °C with a calculated bulk silver conductivity of 15 %, Genes'Ink outperformed Sun Chemical AST 6000 by a factor of ~6.

Table 3: Values of the surface resistivity and the calculated bulk conductivity compared to silver in %

	Sun Chemical AST 6000		Genes'Ink S-C21303	
Sintering Condition	120 °C, 120 min	150 °C, 120 min	120 °C, 120 min	150 °C, 120 min
Surface Resistance [Ω·□$^{-1}$]	0.10 ±.0.035	0.07 ± 0.013	0.03 ± 0.005	0.02 ± 0.004
Bulk Silver Conductivity [%]	1.5	2.4	9.8	15.1

5 Device performance

5.1 Printing & yield

The printing process of screen printing humidity sensors is layout-based divided into three successive parts. After printing and sintering the bottom electrode, the layout of the sensitive micro-composite dielectric layer is printed onto the bottom electrode in a second step and then cured at 120 °C for 5 minutes. The last step is realized by printing the top electrodes. In order to investigate layer properties with correlated device performance, profilometric measurements of each individual layer were realized. In Fig. 5, microscopic analyses and profilometric measurements for a humidity sensor with a triple-printed, sensitive micro-composite dielectric layer and Sun Chemical AST 6000 as electrode conductive material are shown.

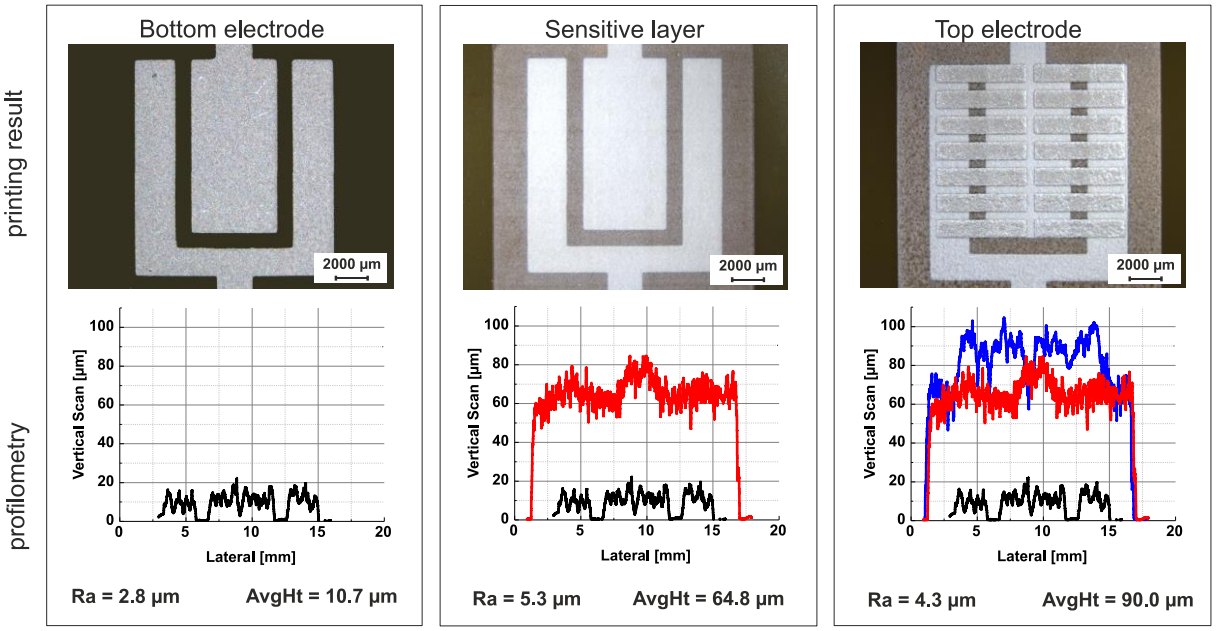

Fig. 5: Microscopic analysis and profilometric measurements of the humidity sensor with triple-printed (3-layer) sensitive micro-composite dielectric layer and electrode material Sun Chemical AST 6000

With an average printed layer thickness of AvgHt = 10.7 µm on flexible Kapton® substrate, Sun Chemical AST 6000 outlines a sufficient layer thickness to provide conductivity at the given screen printing setup. The printing results of this material on a printed water-sensitive micro-composite dielectric layer are slightly different. Here the surface roughness of printed and cured silver material changes.

Reasons for this could be a high roughness of R_a = 5.3 µm on the printing surface, which can be seen from the triple-printed sensitive micro-composite dielectric layers themselves, as well as the influence of the curing dependent porosity of the printed sensitive micro-composite dielectric layer. The inhomogeneity of the printed layer thickness could also cause changed printing results. Due to its capacitance-changing influence, the layer thickness of the printed sensitive micro-composite dielectric layer was investigated with respect to the amount of successive prints for both silver electrode pastes. Table 4 gives an overview of the amount of printed sensitive micro-composite dielectric layers in relation to the average layer thickness, roughness, capacitance and yield of working sensors based on Sun Chemical AST 6000 on one fabricated sheet of sensors.

Table 4 Number of printed dielectric layers in relation to the average layer thickness, roughness, capacitance and yield of working sensors based on Sun Chemical AST 6000 electrodes

Layer Count	AvgHt [µm]	Ra [µm]	Capacitance [pF]	Yield [%]
1	32.2	4.8	-	0
2	44.3	4.2	8.5 ± 1	64
3	71.3	4.3	6.2 ± 1	100

It can be seen that the layer thickness influences not only the capacitance but also drives the yield per printed sheet. While for single printed layers of sensitive micro-composite dielectric materials not a single working sensor could be utilized, for triple-printed sensitive micro-composite dielectric layers all sensors of a single sheet were measurable. One reason for this could be the high surface roughness of Sun Chemical AST 6000, mainly caused by the large particle size distribution which, in the case of thin dielectric layer, could push particles of the printed top electrode through the dielectric layer. In contrast, when Genes'Ink C-S21303 was used as electrode material, no single working sensor could be produced, no matter the amount of layers printed, although the paste system is based on nanoparticles. In order to identify possible failure mechanisms leading to a reduced or inhibited yield, besides optical microscopy, scanning electron microscopy was also applied to prepared sensor cross-sections built with both electrode silver pastes. Fig. 6 shows an overview of both sensor structures, both with triple-printed, sensitive micro-composite dielectric layers.

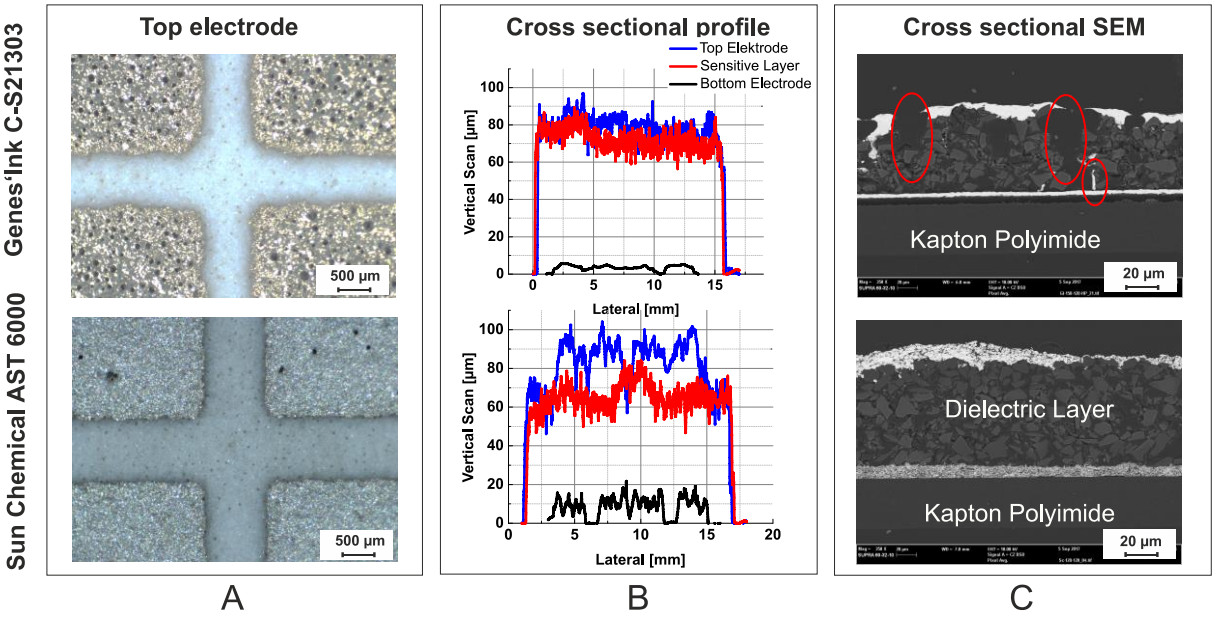

Fig. 6: Overview of sensor builds with triple-printed sensitive micro-composite dielectric layers using microscopy (A), profilometry (B) and cross-sectional SEM analysis (C) for C-S21303 and AST 6000

The porosity of the cured sensitive micro-composite dielectric layers becomes visible when comparing both sensor structures by means of optical microscopy. Black dotted micro air pockets appear on the surface. The reason for this could be drying and curing effects caused by the chosen curing setup in combination with unique curing properties defined by the chosen binder / solvent combination. Additionally, different curing results can be identified between the two silver electrode materials. While Sun Chemical AST 6000 delivers an optically dense coverage of the sensitive micro-composite dielectric layer and exhibits only a few blowholes, the curing of Genes'Ink C-S21303 with the given curing setup leads to a much more blowhole-perforated surface. Additionally, the layer thickness on top of the sensitive micro-composite dielectric layer with Genes'Ink C-S21303 remains visibly thinner after curing compared to Sun Chemical AST 6000. This could be due to the origin of Genes'Inks nanoparticles, but also due to its lower solids content and its different binder / solvent combination. This effect is also represented by the overall layer properties of Genes'Ink C-S21303 when printed on a flexible Kapton® substrate. With a layer thickness of AvgHt = 3.2 µm and R_a = 0.7 µm, the electrode layers printed by Genes'Ink C-S21303 are not only thinner compared to Sun Chemical AST 6000 (AvgHt = 10.7µm), but also much smoother compared to the roughness of Sun Chemical AST 6000 (R_a = 2.8 µm). The reasons for this difference are mainly based on different particle size distributions and solids contents in a fixed printing screen setup. The SEM analysis of the sensor cross-section based on the Genes'Ink structure reveals the relationship between micro blowholes and sensor functionality. In detail, a non-functional sensor based on Genes'Ink C-S21303 exhibits micro blow holes (red circles) and silver electrode material migrated perpendicularly into the sensitive micro-composite dielectric layer. In contrast, such effects are not visible in the cross-section of the functional sensor based on AST 6000. In order to outline a more detailed investigation, focused ion beam analysis (FIB) was applied to emphasize the migration effect of silver into sensitive micro-composite dielectric layer in combination with formation of micro blowholes. The result of FIB analysis is shown in Fig. 7.

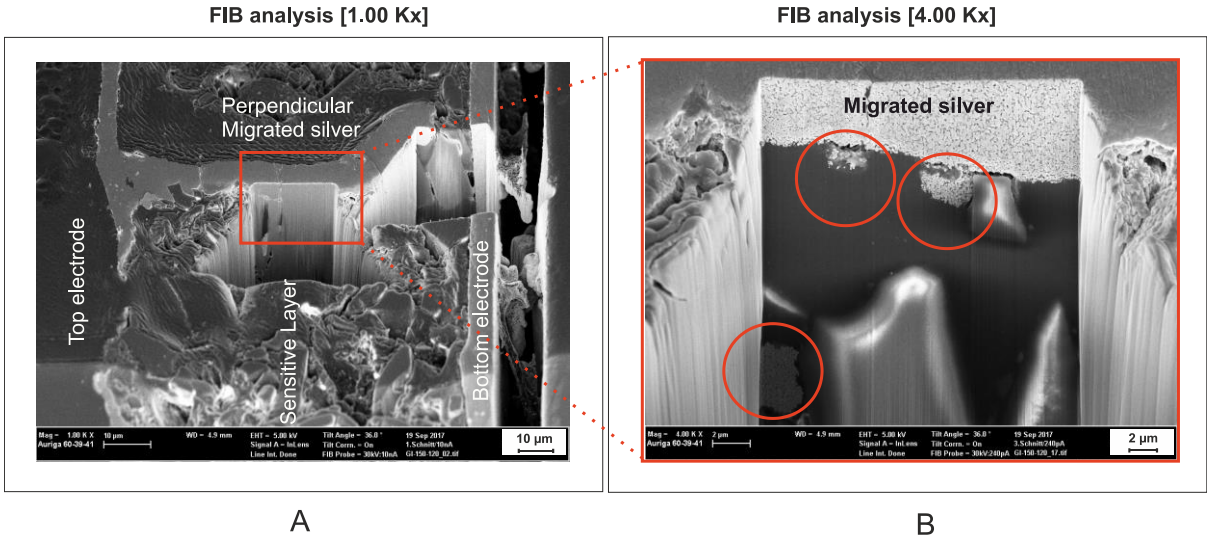

Fig. 7: Migration effect of silver into a sensitive micro-composite dielectric layer in combination with resulting micro blowholes, represented by a cross-sectional SEM (A) and FIB (B)

Fig. 7A shows that perpendicularly migrated silver originating from the printed silver top electrode find its way down to the printed silver bottom electrode. A detailed look at the emerging interface of the FIB process between the top and bottom electrode reveals several areas of migrated silver. This migration effect mainly causes electrical connections between top and bottom electrode, which in turn leads to the non-functionality of the sensor itself. The reasons for such an effect could be based on the porosity of the sensitive micro-composite dielectric layer itself, or chemically compatible binder / solvent combinations between Genes'Ink C-S21303 and customized micro-composite dielectric paste used for the manufacturing of the dielectric layer. Chemical compatibility would cause the chemical dissolution of the already cured sensitive layer, which in turn would support the migration effect of silver itself. The porosity of the sensitive layer could be affected by unfavorable curing step of the sensitive micro-composite dielectric layer, whereby the solvent of the sensitive micro-composite dielectric paste evaporates too quickly, which would in turn cause the solvent to escape from the printed layer by vapor pressure leaving micro blowholes in the dielectric layer.

5.2 Device performance

, Besides the process of humidity measuring procedure, Fig. 8 also shows the change in absolute capacitance values for increasing and reducing actual humidity between 20 % r. h. and 90 % r. h. in combination with average values of humidity. As visible in Fig. 8A measured sensors provided an ascending and descending capacity in dependence of step-wise set positive or negative change in humidity over defined period of time with a phase of stabilization between each step. This behavior is generally an indicator for actual working sensors. In Fig. 8B the characteristic curve of a tested sensor is shown. A hysteresis between ascending change in capacitance and descending change in capacitance becomes visible. With decreasing humidity the sensor takes more time to return to its origin state, what is represented by larger values of capacitance arriving after humidity is returning to a certain value after reaching the maximum humidity/capacitance value before. Main reason for such behavior is slow desorption of water molecules after their absorption, due to an extended network of nanochannels in the porous silica particles.

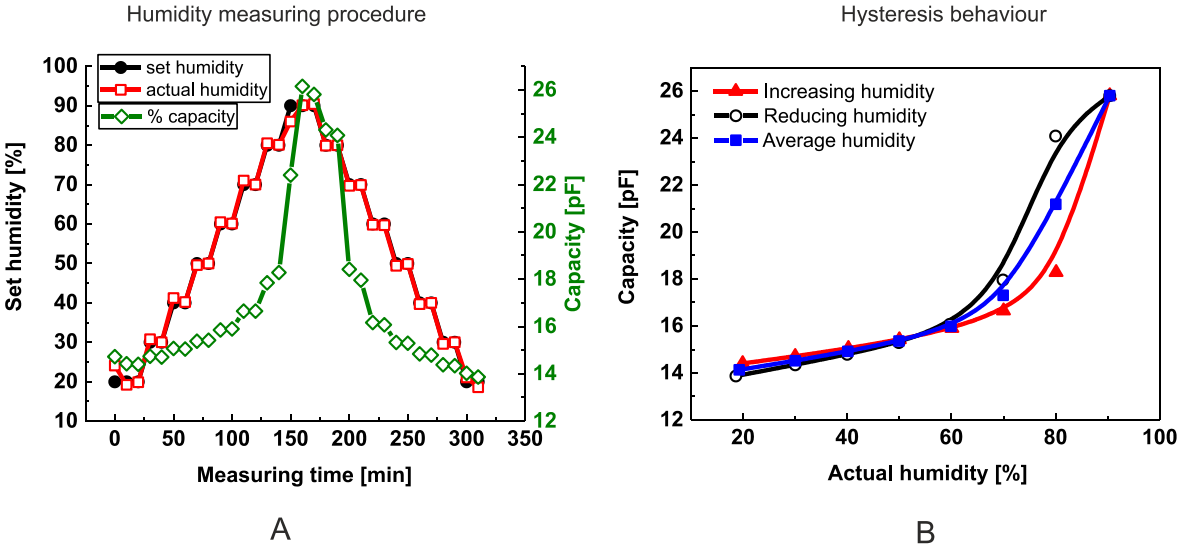

Fig. 8: Process of humidity measuring procedure (A), Change in absolute capacitance values for increasing and reducing actual humidity (B) between 10 % r. h. and 90 % r. h.

6 Discussion and conclusion

The additive manufacturing of humidity sensors produced by screen printing was demonstrated with a three-layer approach based on a sensor's working principle. Additionally, the manufactured sensors were monitored regarding functionality and characterized with respect to sensors hysteresis, which is influenced by the sensor's water molecule absorption and desorption on the sensitive micro-composite dielectric layer itself. The manufacturing of sensitive micro-composite dielectric paste was successfully developed and optimized for screen printing with rheological characterization. Commercially available silver-based paste systems were benchmarked regarding their electronic conductivity and revealed a bulk silver conductivity up to 15 % for a given curing setup. But this three-layer approach places enormous demands on the interaction between the materials involved for the multi-layer build up. Besides wettability, chemical and rheological compatibility plays a more important role for the successful printing of multi-layered humidity sensors than a unique functional property of an electrode material, such as electrical conductivity. This was one reason not to choose the electrically more efficient paste system for the multi-layer build up, but rather the chemically compatible one. This decision was supported by the investigation of the occurring malfunction of printed sensors with help of interface-focused analysis techniques such as FIB. In order to further enhance this approach to the manufacturing setup in terms of the printed sensor performance, the use of multi-materials for the build-up of sensors needed to be optimized with respect to the chemical or rheological compatibility between all materials involved. Furthermore, an increase in sensor capacitance should be addressed by further reducing the layer thickness of the sensitive layer. This would require chemically and rheologically comparable, stable layers in which the interaction at the layer's interface must be excluded and the influence of the functional particle's size must be prevented.

Acknowledgements

This work was carried out within the framework of the Federal Cluster of Excellence EXC 1075 “MERGE Technologies for Multifunctional Lightweight Structures”, which is funded by the German Research Foundation (DFG). The financial support is gratefully acknowledged.

References

[1] L. C. Hollaway, “A review of the present and future utilisation of FRP composites in the civil infrastructure with reference to their important in-service properties,” Construction and Building Materials, vol. 24, no. 12, pp. 2419–2445, 2010. DOI:10.1016/j.conbuildmat.2010.04.062.

[2] A. Zaman, S. A. Gutub, and M. A. Wafa, “A review on FRP composites applications and durability concerns in the construction sector,” Journal of Reinforced Plastics and Composites, vol. 32, no. 24, pp. 1966–1988, 2013. DOI:10.1177/0731684413492868..

[3] B. C. Ray and D. Rathore, “Durability and integrity studies of environmentally conditioned interfaces in fibrous polymeric composites: Critical concepts and comments,” (eng), Advances in colloid and interface science, vol. 209, pp. 68–83, 2014. DOI:10.1016/j.cis.2013.12.014.

[4] H. Farahani, R. Wagiran, and M. N. Hamidon, “Humidity sensors principle, mechanism, and fabrication technologies: A comprehensive review,” (eng), Sensors (Basel, Switzerland), vol. 14, no. 5, pp. 7881–7939, 2014. DOI:10.3390/s140507881.

[5] T. Seider et al., “Highly-Sensitive Humidity Sensors for Condition Monitoring of Hybrid Laminates,” MSF, vol. 825-826, pp. 579–585, 2015. DOI:10.4028/www.scientific.net/MSF.825-826.579.

[6] H. Zhao et al., “Drawn on Paper: A Reproducible Humidity Sensitive Device by Handwriting,” (eng), ACS Appl. Mater. Interfaces, vol. 9, no. 33, pp. 28002–28009, 2017. DOI:10.1021/acsami.7b05181.

[7] F. Ebert et al., “Integration of Humidity Sensors into Fibre-reinforced Thermoplastic Composites,” Procedia Technology, vol. 26, pp. 207–213, 2016. DOI:10.1016/j.protcy.2016.08.028.

[8] A. Rivadeneyra et al., “Printed electrodes structures as capacitive humidity sensors: A comparison,” Sensors and Actuators A: Physical, vol. 244, pp. 56–65, 2016. DOI:10.1016/j.sna.2016.03.023.

[9] C. Gaspar, J. Olkkonen, S. Passoja, and M. Smolander, “Paper as Active Layer in Inkjet-Printed Capacitive Humidity Sensors,” (eng), Sensors (Basel, Switzerland), vol. 17, no. 7, 2017. DOI:10.3390/s17071464.

[10] J.-V. Voutilainen, T. Happonen, J. Hakkinen, and T. Fabritius, “Screen-Printed Remotely Readable Environmental Sensor Pair,” IEEE Sensors J., vol. 16, no. 10, pp. 3523–3531, 2016. DOI:10.1109/JSEN.2016.2532383.

[11] G. Dubourg et al., “Fabrication and Characterization of Flexible and Miniaturized Humidity Sensors Using Screen-Printed TiO_2 Nanoparticles as Sensitive Layer,” (eng), Sensors (Basel, Switzerland), vol. 17, no. 8, 2017. DOI:10.3390/s17081854.

[12] A. Rivadeneyra et al., “Asymmetric enhanced surface interdigitated electrode capacitor with two out-of-plane electrodes,” Sensors and Actuators B: Chemical, vol. 254, pp. 588–596, 2018. DOI:10.1016/j.snb.2017.07.141.

[13] R. Alias and S. Mohd, “Rheological Behaviors and Their Correlation with Printing Performance of Silver Paste for LTCC Tape,” in Rheology, J. de Vicente, Ed., Rijeka: InTech, 2012. DOI:10.5772/35004.

[14] J. Phair and A. F. J. Kaiser, “Determination and assessment of the rheological properties of pastes for screen printing ceramics,” in Nordic Rheology Conference, vol. 17, Annual transactions The Nordic Society, Reyjavik, Iceland, 2009, pp. 177–181.